Experimental Investigation on a 3D Wing Section Hosting Multiple SJAs for Stall Control Purpose

Experimental Investigation on SJAs Stall Control

Author, co-author (Do NOT enter this information. It will be pulled from participant tab in MyTechZone)

Affiliation (Do NOT enter this information. It will be pulled from participant tab in MyTechZone)

ABSTRACT

The control of the flow over aerodynamic shapes in order to achieve performance enhancements, such as improved aircraft maneuverability, has been a lively area of research for last two decades. Active flow control can produce significant performance improvement when combined in a closed-loop control system. Synthetic jet actuators (SJAs) are devices able to interact actively with the flow around a hosting structure by providing ejection and suction of fluid from an orifice. The research presented in this paper concerns the implementation of zero-net-mass-flux SJAs airflow control system on a NACA0015, low aspect ratio (LAR) wing section prototype developed by Clarkson University under the Advancement of Intelligent Aerospace Systems (AIAS) AFOSR Grant FA9550-09-1-0051. Two arrays of custom made SJAs, installed in the proximity of the leading edge and flap of the wing section, make up the actuation system. The sensing system consists of eleven acoustic pressure transducers distributed in the wing upper surface, an accelerometer placed in proximity of the wing center of gravity and a six-axis force balance. A dSPACE hardware connected to the software environment Matlab / Simulink / Control Desk complete the test architecture. Wind tunnel experiments, on the uncontrolled wing, are primarily performed for system identification purpose. The open-loop control of the wing is implemented and tested, obtaining a stall postposition of about 2.8 degrees of angle of attack. A strategy based on the comparison of the mean pressure chord-wise distributions, senses by the acoustic pressure transducers for different angles of attack, on the wing upper surface is adopted to characterize the forthcoming boundary layer detachment. This allows for triggering the closed-loop control in stall proximity only for energy saving purpose. Pertinent results and discussion are provided.

INTRODUCTION

The boundary layer active control as means for wing stall post-position has been the main objective of the investigation carried out at Clarkson University under the Air Force Office of Scientific Research (AFOSR) grant number FA9550-09-1-0051.

Years of research led to the closed-loop control experimental campaign over a low aspect ratio (LAR) wing section, at low Reynolds numbers. The continuously growing efforts on the topic, which characterized the last two decades of research in aeronautical field, led to the definition of several strategies to perform active flow control over finite wings [1]. The obvious expected result is the improvement of aircraft aerodynamic performance at relatively low costs with significant energy savings [2]. To this purpose, a strip of Synthetic Jet Actuators (SJAs) distributed in arrays across the wingspan [3] can constitute a viable actuation system. Their small size, ease of working operation and low costs, make them the favorite candidate for experimentation purpose. Some examples of experimental investigation, conducted on other wing assemblies to study the effective aerodynamic performance enhancements are available [4], [5], [6], [7]. As the use of two arrays of SJAs located in proximity of the leading edge and of the flap shoulder resulted in satisfactory outcomes, [8], [9], the same configuration will be maintained in the presented work. In addition, the application on a LAR wing and at low Reynolds number is particularly stimulating in the present aeronautical scenario, characterized by a wide development and production of small/micro unmanned aerial vehicles (UAVs/MAVs), [10]. Finally, the future extension of these technologies to large-scale air vehicles is very attractive as far as fuel consumption and pollutants' emissions reductions are concerned [11]. Short take-off and landing distances and drag reduction, contributing to lower thrust requirements are main contributing factors to next generation of aircraft greening operation. Recently a research team has succeeded in eliminating the hinged control surfaces by the use of SJAs on a UAV leading edge wing [12], [13]. Applications of SJAs as hingeless wing control have been also performed in innovative configurations. These consist of SJAs located in the wing upper and lower surfaces in proximity of the trailing edge, and integrated with Coanda effect surfaces [14]. The encouraging results in terms of lift, drag and pitch moment characteristic improvement paved the way for further investigations. Symmetric airfoils have been used extensively for SJAs effectiveness validation purpose. This is justified by the easier manufacturing process and the promising application of these devices on small scale and slow speed air vehicle [15]. Cases of SJAs application on non-symmetric-airfoil-wing are also available in literature. A case in point is [16], where a series of piezo-electric driven SJAs, located at the 12% of the chord on a wing, is employed

to control the airflow around a NACA63$_3$018 airfoil, at low Reynolds number conditions. In this case, the jets interact with the surrounding flow field by eliminating, or simply reducing, the upper surface separation bubble with consequent lift-drag ratio improvement. Moreover, further studies pointed out the detrimental effect of the Reynolds number on the SJAs performance [16]. All of the cited phenomena have been confirmed and are in agreement with the major outcomes of the presented experimental investigation.

The presented research work intended to experimentally investigate and validate the efficacy of previously designed and optimized SJAs on a LAR wing. The already complex task is intensified by the interaction between the synthetic jets and the complex three-dimensional flow field, which characterizes LAR wings [17]. A closed-loop control architecture is investigate to provide useful insights for future application on complete air vehicles.

The rest of the paper is organized as follows: firstly, an explanation of the physics behind the SJAs functioning and the stall post-position is given and the custom-made SJAs design is presented. The following section provides an overview of the hardware-software configuration employed. SJAs' parameters' tuning process that led to the more effective combination in terms of stall post-position is the subject of next section. The open-loop and closed-loop experiment and results are presented in subsequent sections. Finally, summary and conclusions are presented in the closing statements.

SYNTHETIC JET ACTUATORS AND FLOW SEPARATION IN LAR WINGS

In recent decades synthetic jet actuators have been widely studied to perform the flow control around aerodynamic shapes. They belong to the fluidic active control devices category and in particular they are defined as zero-net-mass-flux actuators: they are able to create the synthetic jet by a mechanism of periodic fluid suction and injection from the boundary layer. The main elements of a SJA assembly are:

- A vibrating diaphragm;
- An housing (actuator's cavity);
- An orifice slot.

The air access point to entry and egress the actuator cavity is the orifice that connect the actuator's chamber with the external environment. The shape and orientation of the orifice define the energy transfer condition into the boundary layer, and therefore must be properly designed. The SJAs devices are identified by a solid and confined assembly that does not require any dedicated air supply system. Only the electrical wires carrying the command signal represent the additional cumbersome element. The actuator active component is a generally a piezo-electric membrane, located at the bottom of the chamber. The synthesis of the air jet is obtained by electrically forcing the membrane vibration and it is also related to the chamber resonance condition, known as Helmholtz frequency [19]. The physics behind the SJAs functioning during each membrane oscillation period is hereafter shortly described. The air egress is obtained by the cavity volume reduction that occurs when the piezo-electric diaphragm moves toward the orifice. The inner higher pressure produce the air jet expulsion through the orifice. This results in a shear layer between itself and the surrounding fluid, which is related to the flow separation inducted by the air jet emission. The shear layer vorticity rolls up, thanks to its own momentum, to form a vortex ring which starts to move downstream carried by the air flow. Vice versa, when the diaphragm is deformed to result in a chamber volume increment, the air suction into the cavity occurs forced by the inner lower pressure. At this point, the vortex ring previously created is sufficiently distant from the orifice to prosecute its path. This process associates a non-zero-mean-momentum flux to a zero-net-mass system. It results in the creation (synthesis) of jets that cause a train of vortex rings obtained by properly disturbing the boundary layer. The synthetic jet actuators employed in the present research have been previously designed and built at Clarkson University under the same research project, [8] and [19]. The orifices orientation has been optimized in order to create air jets with an injection angle of 30 degrees. In addition, the optimization process has concerned all the other parameters defining the SJAs geometry, such as the shape, dimensions and size of the cavities, and electrical characteristics of the piezo-electric membranes. The actuators' active elements are piezo-electric diaphragms composed by a brass round of 32 mm of diameter and 0.10 mm of thickness and a piezo-ceramic PZT-5h round with a diameter of 32 mm and a thickness of 0.22 mm. The active element is similar for the leading edge and for the trailing edge actuators. However, the front and the back lines of actuators differ for the shape, the cavity dimension and for the housing design (Figure 2). This is mainly due to the different shape and thickness of the airfoil in those positions.

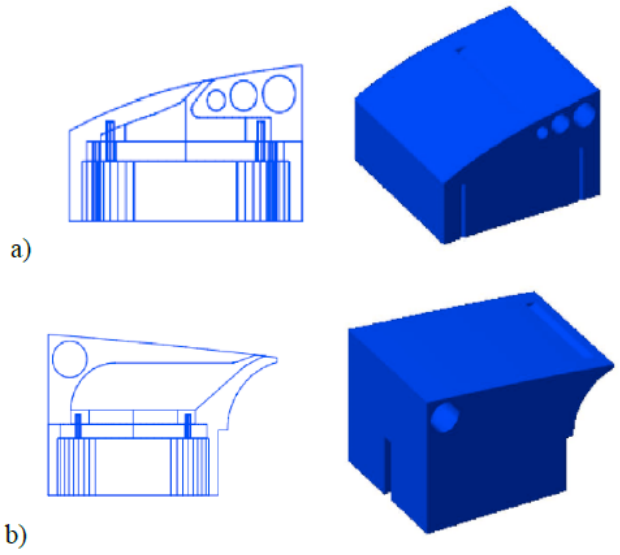

Figure 1 - Clarkson University SJAs assemblies (a) Leading edge (b) Trailing edge [19]

In Figure 1 the exploded view of the custom-made leading edge SJAs is reported. All the actuator components are illustrated apart and in their mounting sequence. The assembly includes two aluminum compression rings (top and bottom), which clamp the piezo diaphragm, an aluminum O-ring which holds the piezo in place between the compression rings, a neoprene washer and a plastic housing. The actuators' cavities have a volume of 4650 mm^3 and 10738 mm^3 for the leading edge and for the flap shoulder positions, respectively.

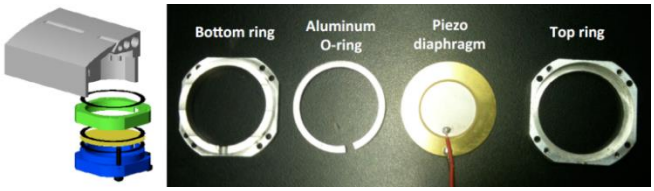

Figure 2 - Schematic view of the LE SJAs assembly (left) and SJAs main elements (right) [19]

The optimal SJAs working condition has been obtained by driving the actuators with an electric sine wave signal and performing a frequency sweep test. The jets peak velocities have been identified in correspondence of 1000 Hz and 1100 Hz for the flap shoulder and the leading edge SJAs arrays respectively [19].

In the present work the two arrays of SJAs are driven by the same sine wave signal, resulting in an optimal working frequency of 1050 Hz, as better explain in the "Parameter Determination" section. In addition, a sensitivity analysis concerning other parameters, such as the duty cycle and the signal mean voltage, has been performed to optimize the SJAs for stall postposition purpose. As already mentioned, the described SJAs strips have been installed in a LAR finite wing. This choice allows the investigation of the SJAs effectiveness with complex flow field as the one deriving from this type of wing. The aerodynamics in this configuration is three-dimensional and exhibits several correlated phenomena of interest such as the wing-tips vortices, the separation and reattachment of the boundary layer, the laminar to turbulent transition and the formation of the separation bubble on the upper surface [20]. For example, the wing-tip vortices interest a great portion of the wing, because of its short span, and one of the main effects is the delay of the flow separation from the upper surface, compared to the two-dimensional airfoil [21], [22]. Moreover, at low Reynolds numbers, the laminar separation bubble is a well-known phenomenon caused by the strong adverse pressure gradient experienced by the fluid lapping the wing upper surface. The laminar boundary layer, which characterizes the low Reynolds number flow tends to detach, also at relative low angles of attack; once separated it still remains laminar for a small portion of the chord, but being very sensitive to disturbances, it turns turbulent (laminar to turbulent transition); this evolution affects a zone called transition region. Studies have been conducted on the observation of the evolution phases of the laminar separation bubble [23]. The turbulent flow is more energetic and reattaches to the wing surface delimiting the laminar separation bubble area. The laminar separation bubble influences the LAR wing aerodynamic in terms of drag increase and lift distribution disturbances. Increasing the angle of attack the separation bubble firstly moves upstream, towards the leading edge, until the adverse pressure gradient becomes too severe causing the bubble to burst and leading to the stall of the wing. All the described phenomena have been experienced during the test and will be described in the proper section.

EXPERIMENTAL SET-UP

Wing Section

The low aspect ratio ($AR = 1.33$) wing section employed for the proposed experiment has been designed and built at Clarkson University, and is shown in *Figure 3*. It has a span of 40 cm, chord length of 30 cm and a NACA 0015 airfoil. The wing assembly is modular and composed by three parts to guarantee maintainability and reliability. The body material is 6061 aluminum alloy. The two arrays of SJAs (10 per line) are located at 10% and 65% of the chord length. The wing is equipped with 11 PCB 103B01 high sensitivity acoustic ICP pressure sensors. They are grouped as follows: eight sensors in the main wing body (located between the 19% and the 45% of the chord length) and three inside the flap (between the 75% and 82% of the chord length). They are located underneath eleven pinhole orifices of 1.2 mm of diameter on the upper surface of the wing section. The line of pressure sensors is positioned at 14.4 cm from the right wing tip.

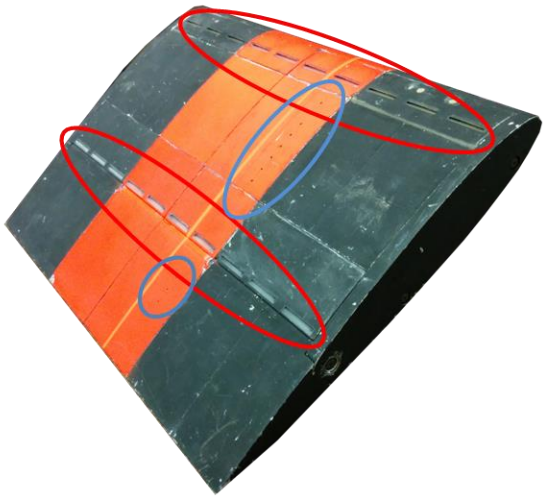

Figure 3 - Wing Assembly, red rounded: SJAs Arrays, blue rounded: Acoustic Pressure Transducers

Hardware and Software

The experimental set-up is finally integrated with the following components:

Hardware

- 2 Control Computers
- dSPACE DS1103 System
- Trek350A Piezo Driver / Power Amplifier
- 3 4-Channel PCB Signal Conditioner

Software

- Matlab / Simulink / Control Desk
- Labview

The dSPACE DS1103 system has two components: the real-time processor PPC Controller Board and the CP1103 Connector Panel. It has been used to create and send the control command signal to the SJAs and to receive at the same time data from the 11 pressure transducers. In this investigation, the models are developed using Matlab / Simulink and the DS1103 Real-Time-Interface (RTI) interact real-time with them. The second control computer, which is connected to the force balance system through a National Instruments (NI) data acquisition system (DAQ), uses Labview software. The NI DAQ system includes the SCXI-1000 and NI PCI-6221 cards, which provide 2 analog out, 8 analog input and 24 digital input / output signals; the motion interface box UMI7764 is plugged to the control computer. A Labview code is used to control the pitch motion of the model inside the wind tunnel and to get the force data from six analog channels simultaneously.

The experiment has been run in the Clarkson University High Speed (CUHS) wind tunnel facility. It is open-circuit, suction type wind tunnel and the maximum airspeed is about 70 m/s. The force balance system (FBS) is a six-axis AEROLAB device. The balance sting is supported by two motion bars which control the motion of the wing section in the pitch plane. The motion bars are driven by an accurate step motor. The wind speed is measured by the CPG Digital Pressure Gauge 2500 instrument (Mensor Corporation) connected to the pitot tube properly located inside the wind tunnel. The entire experiment set-up architecture is shown in Figure 4 and Figure 5, enlighting separately the input (from control board to actuators) and the output (from sensor to control board) signal path respectively.

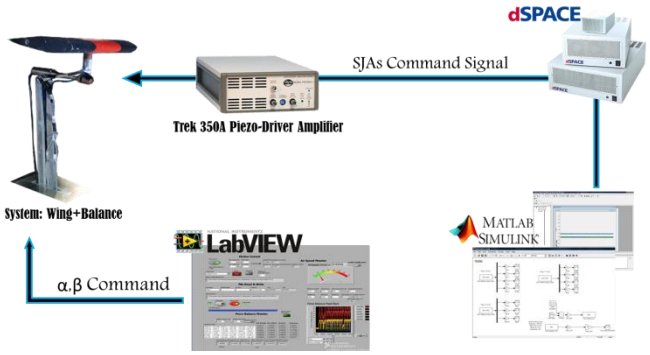

Figure 4 - Experimental Set-up, System Inputs

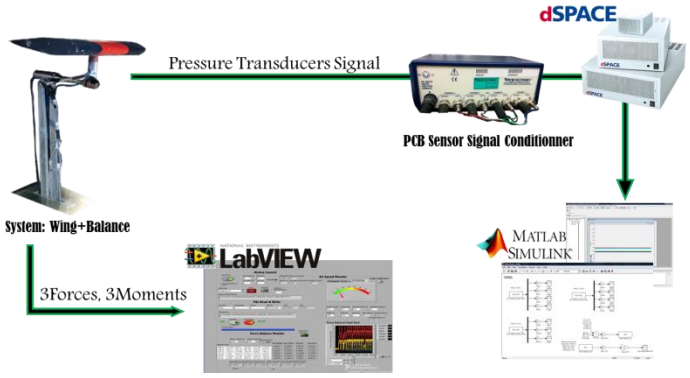

Figure 5 - Experimental Set-Up, System Outputs

It is worth pointing out that the working frequency of the actuators and the sensors is the same as they are interfaced to the running code on the dSPACE system processor. The Labview code interfaced to the force balance system has its own settings and working frequency.

PARAMETERS DETERMINATION

The interaction of the SJAs with the surrounding flow field is strictly linked to the type of power signal that feeds the actuators [24]. A preliminary open-loop analysis to determine the power signal characteristics is then required. The experimental parameters tuning process starts from a reasonable configuration and sweeps a large range of conditions until the best trade-off is found. For given signal shape, which is a sine wave in this case, the following parameters must be optimized:

- Frequency
- Duty Cycle
- Mean Voltage (Bias)

The sine wave amplitude, which usually requires optimization as well, is fixed to $5\,V$ in the proposed application because of the employed piezo membrane limitation, to preserve structural integrity. The optimization process is detailed for each parameter in the following subsection. The initial condition is: bias of $25\,V$, frequency

of 460 Hz and Duty Cycle of 0 Hz; the tuning sequence is: firstly the sine wave frequency is determined and locked, secondly the duty cycle frequency as well, and as last the signal voltage bias is optimized. The entire set of test is conducted at the same wind tunnel speed, $U_\infty = 5\ m/s$. The objective function of the entire optimization process is the wing stall angle of attack, α_{stall}.

Sine Wave Frequency

The first test is performed by a continuous actuation of the SJAs with a single signal for both arrays. The $C_L - \alpha$ curve is obtained by means of the six-axis force balance for each sine wave frequency and then compared.

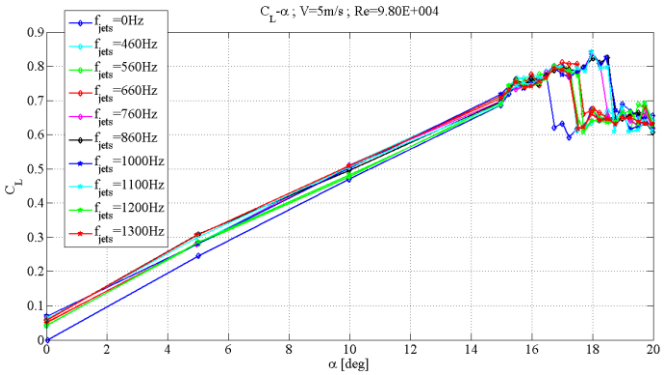

Figure 6 - Lift coefficient vs. AOA for different sine wave frequencies in the range [0Hz-1300Hz], @25±5 V , U=5 m/s

As shown in Figure 6, increasing the power signal frequency from $0Hz$ to $1300Hz$ a nonlinear proportional trend with the resulting α_{stall} is noticed. The stall angle of attack reaches its maximum value in correspondence of the frequency range enclosed between 860 Hz and 1100 Hz, while it is smaller for lower and higher power signal frequencies. Narrowing the frequency band between 1000 Hz - 1100 Hz the optimal solution is found to be 1050 Hz.

Duty Cycle Frequency

The duty cycle frequency is obtained by multiplying a square wave, oscillating between zero and one, to the pure sine wave. Its employment allows a finest tuning of the power signal for stall postposition purpose. Regulating the square wave frequency results changing the activation time of the power signal. For the previously investigated decoupled configuration (two different power signal for the two SJAs lines) the best trade-off has been found to be in the range $0Hz - 200Hz$ [19]. Consequently, the same range of duty cycle frequencies has been experimentally investigated in the proposed coupled configuration (one power signal for both SJAs lines). As expected and shown in Figure 7, different duty cycle periods provide different effects, beneficial only when able to let the jets frequency better interact with the proper frequency of the flow field surrounding the wing. For example, applying a duty cycle with a frequency of $f_{DC} = 10Hz$ results in a detrimental effect of about one degree with respect to the pure sine wave case. Instead, while a duty cycle with a frequency of $f_{DC} = 50Hz$ does not produce any effect, $f_{DC} = 100Hz, 160Hz$ and $200Hz$ increase α_{stall} of about one degree. The optimal solution, finally implemented in the control system and kept constant for the rest of the experimental campaign, is found to be $f_{DC} = 160Hz$.

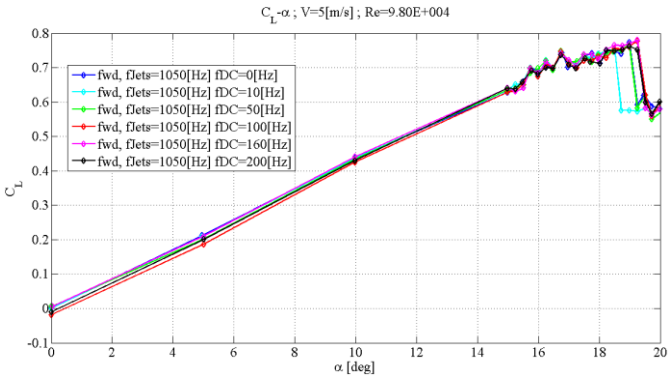

Figure 7 - Lift coefficient vs. AOA for different Duty Cycle frequencies in the range [0Hz-200Hz], @ f jets=1050Hz

Sine Wave Mean Voltage

The power signal mean voltage directly affects the static position of the piezo diaphragm and so its excitation level. Despite previous research on the decoupled configuration, suggested a bias voltage of 25 V for the power signal, it has been attempted to increase the voltage bias up to $30V$, which is the maximum tolerated by the piezo membrane. The beneficial effect deriving from the new setting is shown in Figure 8. The lift coefficient drop is still postponed of about one degree, which makes the overall $\Delta\alpha_{stall} \approx 3$ degree from the initial clean configuration. Even if the objective α_{stall} does not appear to be heavily affected by this parameter, the higher lift coefficient suggested keeping the new setting in the experiment prosecution.

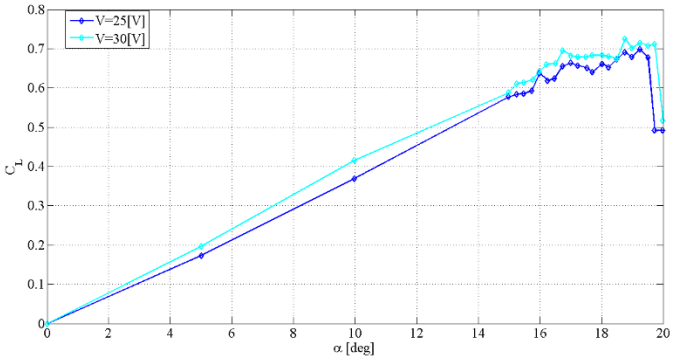

Figure 8 - Lift coefficient vs. AOA @U=5 m/s, for different sine wave mean voltages: V=25±5 V; V=30±5 V

Finally, the optimal configuration to delay stall separation, for the wing-SJAs architecture under investigation, is summarized in Table 1.

Table 1 - SJAs sine wave command signal parameters

Mean value [V]	**30**
Amplitude [V]	**5**
Frequency [Hz]	**1050**
Duty Cycle frequency [Hz]	**160**

WIND TUNNEL TESTS AND EXPERIMENT RESULTS

Wind Tunnel Test

The experiment main purposes are: to validate the optimization process results; to derive the entire set of aerodynamic coefficients in the longitudinal plane for control algorithm development purpose; and to characterize the flow field above the wing in stall proximity by pressure transducers for online real-time active flow control operations. Accordingly, the wind tunnel speed is maintained constant to the optimization value $U_\infty = 5\ m/s$. A sensitivity analysis to the wind speed variation has been also conducted to verify the efficacy of the jets in off-design condition, in particular up to $U_\infty = 10\ m/s$. According to the laboratory environmental conditions, the Reynolds number has thus been varied from $9.53 \cdot 10^4$ up to $1.89 \cdot 10^5$, for $U_\infty = 5\ m/s$ and $U_\infty = 10\ m/s$ respectively. The Reynolds number is obtained using the dynamic pressure information provided by the digital pressure gauge connected to the pitot tube: for each angle of attack the measurements are averaged and the resulting value is employed to compute the averaged Reynolds number, $\overline{\mathrm{Re}}$. Results for $U_\infty = 5\ m/s$ are shown in Figure 9 and Figure 11. The aerodynamic improvement obtained by the SJAs actuation confirms the optimization process results and consists of a lift coefficient increment of $\Delta C_{L_{max}} \approx 0.06$ and stall angle of attack postponement of $\Delta\alpha_{stall} \approx 3\ deg$. The jets seems to affect the wing aerodynamics also in terms of C_{L_0}, whereas C_{L_α} is maintained constant. However, this effect does not appear in Figure 9Figure 11 at higher wind speed. Therefore, the C_L line upward translation should be probably be considered as a measurement error due to the very low Re. In addition, Figure 11 shows a noticeable increment in the clean wing $C_{L_{max}}$ and a smaller effect of the SJAs at $U_\infty = 10\ m/s$. These phenomena are due to the wing-tip vortices of three-dimensional flow field that strongly affects the lift especially for a LAR wing configuration [17]. The tip vortices extend over the wing upper surface for a large portion of the total wing area and their action become the main mechanism for the lift generation. At the same time, the vortices impact the wing upper surface impairing the underlying jets effect. The reduced gap between the blue and magenta lines in Figure 9 and Figure 11 demonstrate the loss of efficacy consequent to the Reynolds number increment.

A similar behavior is observable in the drag coefficient measurements, as reported in Figure 10 and Figure 12. The SJAs' main effect as far as the drag coefficient, C_D, is concerned consist of lowering the drag across the entire range of angles of attack and postponing the drag abrupt increment due to flow separation. Both effects are reduced at higher Reynolds number. This is noticeable by the narrower gap between the two lines in Figure 12. The SJAs' drag reduction effect has different physical explanation depending on which α region is concerned. In fact, in the stall region the aerodynamic improvement is related to the flow energy increment in terms of momentum due to the SJAs' operating principle. Whereas, for smaller α the jets' orifice orientation angle, $30\ deg$, motivates the drag reduction by a resulting positive net force in the wind direction. Furthermore, the drag coefficient is higher when the SJAs are actuated in the post-stall region at higher Reynolds number, Figure 12. In fact, the swirling flow field, which characterizes the wing upper surface aerodynamics in the post-stall condition, seems to be amplified by the synthetic jets. However, simultaneously the post-stall C_L drop is less severe, as shown in Figure 11. Further studies are require to evaluate the convenience of keeping the SJAs actuated after the wing stall occurrence.

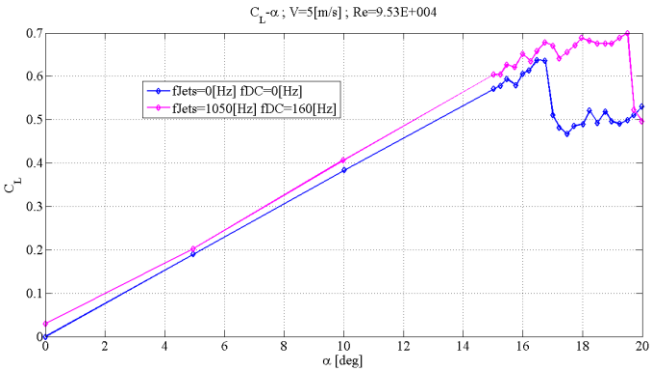

Figure 9 - Lift Coefficient vs. AOA, Actuated and Unactuated Configuration @ 5 m/s

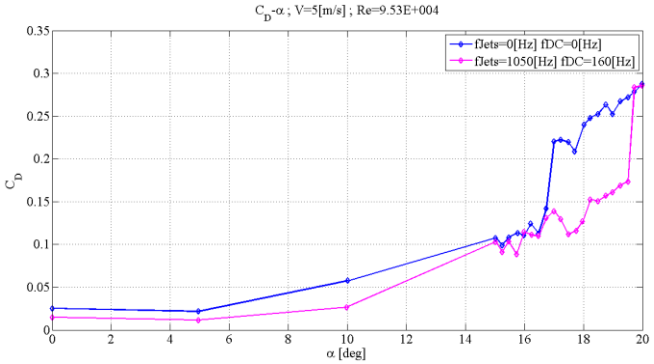

Figure 10 - Drag Coefficient vs. AOA, Actuated and Unactuated Configuration @ 5 m/s

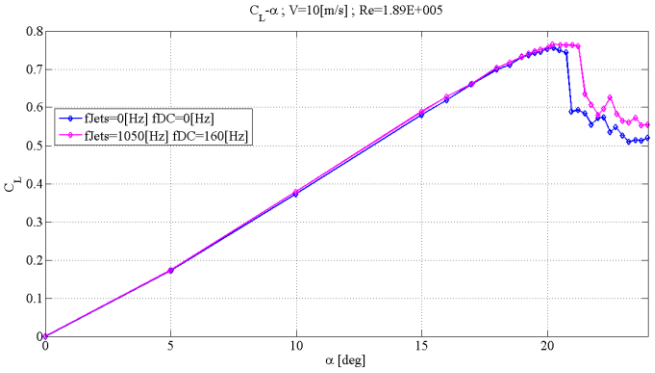

Figure 11 - Lift Coefficient vs. AOA, Actuated and Unactuated Configuration @ 10 m/s

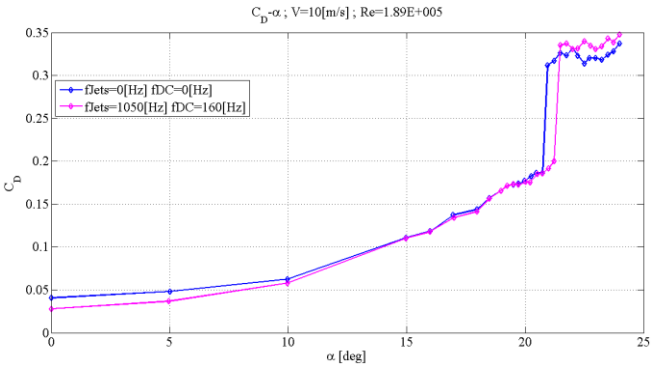

Figure 12 - Drag Coefficient vs. AOA, Actuated and Unactuated Configuration @ 10 m/s

Pressure Data Analysis and Controller Trigger Condition

The major task of the proposed research is to characterize the presence of the stall on the wing upper surface in terms of pressure distribution. Despite its accuracy, the force balance measurement cannot be available on real wing and the definition of an alternative way to sense the incoming stall is necessary. Acoustic pressure transducer are a suitable choice both for wind tunnel experiment and real-world application. For this reason, a sensing system based on acoustic pressure transducers has been designed and installed in the LAR wing under investigation as mentioned in the "Experiment Set-up" section. The test basically consist of recording pressure data for each AoA, from $\alpha = 0°$ up to $20° > \alpha_{stall}$, and processing the data through different methodologies. Data from the acoustic pressure transducers are sampled at a frequency of $f_S = 8\,kHz$. For each angle of attack a recording of 30 sec is taken for each sensor after 15 sec of waiting time after the balance motion to make sure the aerodynamic transient phenomena would not affect the measurements. Data recordings from the eleven pressure transducers have been analyzed with different methodologies in the attempt of finding a signature in the readings to be used as trigger for the active SJAs control board. A feedback signal for a binary, ON/OFF, control law is the main task of this part of the experiment. Firstly, a study over the pressure fluctuation intensities has been conducted. The RMS of the pressure signal time histories can be found as,

$$p_{RMS} = \sqrt{\frac{1}{N}\sum_{n=1}^{N} p_n^2} \qquad (1)$$

where N is the number of samples of each recording and p_n is the n-th pressure value sensed by the transducer. Before computing the RMS, the time histories are de-trended by subtracting the mean value of the entire thirty seconds time histories. The collected data for each pressure transducer have been analyzed in terms of RMS across the chord length and for each angle of attack. The main outcomes are the following:

- Even with wind tunnel and SJAs deactivated, the fluctuations' intensity is not zero because of the working environment noise;
- SJAs activation without wind results in a noticeable increase of the pressure fluctuation intensities due to their own noise;
- Activation of the wind tunnel fan, to obtain $U_\infty = 5\,m/s$ in the test chamber, produces an even higher noise level, which covers the aerodynamic fluctuations' contribution.
- Due to these environmental noise signatures, it has not been possible to identify any kind of signature of the RMS pressure distribution related to the actual angle of attack of the wing.

Secondly, an analysis in the frequency domain has been conducted computing the Magnitude Squared Coherence (MSC) between the sensors' time series data. This is based on the computation of the cross and auto spectral densities of different sets of data and indicates the correlation between the frequency content of different sets of data. In this application, the coherence function has been applied aiming to compare sensors' power spectral densities between them. This approach has been attempted both for SJAs activated and deactivated configuration to find an overall spatial sensors' correlation across the chord length. The results of this analysis have revealed that sensors' signal are correlated in pairs or triplets at the same relative distances, as reported in Table 2. In addition, the frequency range in which the coherence value is higher is always about $[0Hz - 100Hz]$, for all the related sensors.

Table 2 - MSC Analysis Results

Sensor n.	***Coherent Sensor n.***	***Distance between the couple of sensors***
wing 1	wing 5, flap 1	4.40cm, 16.67cm
wing 2	wing 6, flap 2	4.40cm, 16.67cm
wing 3	wing 7, flap 3	4.36cm,16.65cm
wing 4	wing 8	4.40cm
wing 5	flap 1	12.27cm
wing 6	flap 2	12.26cm
wing 7	flap 3	12.29cm

This result suggests that the flow structure on the wing upper surface is characterized by a vorticity pattern whose macro scale length is about $4\,cm$. However, this interesting information about the flow field structure across the wing could not be easily used as signature of the approaching stall. In fact, it is not easy to relate the vortex scale to the angle of attack variation before the stall occurrence. Instead, the trigger condition for the incoming stall has been found analyzing the mean pressure level with respect to its chord-wise distribution. In Figure 13 the normalized mean pressure distributions across the chord length are shown.

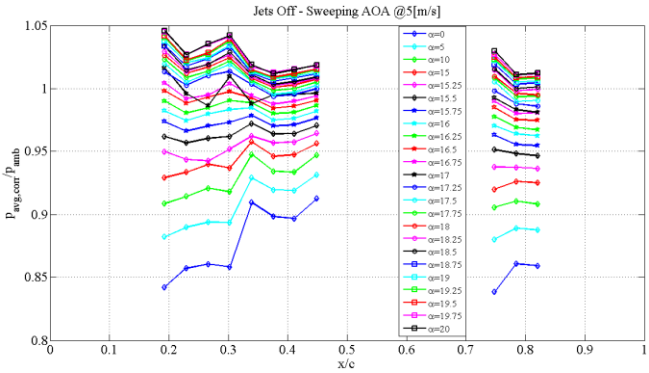

Figure 13 - Mean pressure chord-wise distribution sweeping AOA

Sweeping the angle of attack domain of interest, the pressure distribution across the wing body (pressure transducers one to eigth) exhibits a trend inversion, being almost leveled when stall occurs. For a better understanding of the slope changing phenomenon a linear regression is perfomed on the recorded data (Figure 14). It is worth pointing out that this operation, here in post processing, would be feasible also in a real-time real-world application. From Figure 14, the pressure trend in the wing body transducers changes slope sign between $\alpha = 15.75$ degrees and $\alpha = 16$ degrees, which is slightly before the stall occurence according to the force balance results. It must be noticed that for $\alpha > \alpha_{stall}$ the averaged pressure distributions are below $p_{avg}/p_{ext} = 1$, which describes the suction region on the wing upper surface. For higher angle of attack, $\alpha > 15$ degrees, a pressure drop is observed, in particular as far as the first four sensors are concerned. This phenomenon should be related to the *separation bubble* which affect airfoils typically at low Reynolds number [23]. Moreover, the pressure tends to a uniform leveled distribution, that is the external environmental pressure value when $\alpha \approx 16.75 \,/\, 17$ degrees is reached. This is in agreement with the stall physics of the flow detachment related to the lift drop. Flow visualization by PIV, previously made on the same wing model [19], proves the presence of vortices in the the flow field for these AoA conditions. The vortex impact on the wing upper surface justifies the $p_{avg}/p_{ext} > 1$ values in pressure transducers after the stall occurrence (Figure 13).

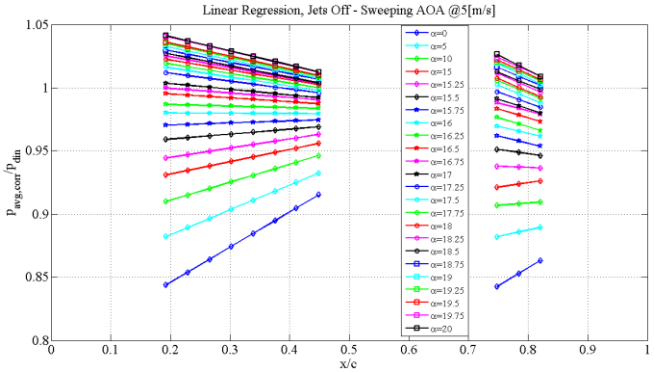

Figure 14 - Linearized mean pressure chord-wise distribution sweeping AOA

CLOSED-LOOP CONTROL STRATEGY

A closed-loop control scheme for the automatic activation of the SJAs arrays in order to postpone the stall, and avoiding continuous functioning strategy, is presented in this section. The objective is to prove the possibility of actuating the synthetic jets only when required without performance loss, with potential energy savings. The control scheme is based on an angle of attack feedback signal read directly from the force balance encoder. The dSPACE real-time interface uses the feedback signal as input to trigger the actuation block in the Simulink control scheme. The closed-loop experiment wind speed is always $U_\infty = 5\,m/s$ for sake of consistency. The control logic is implemented in order to activate the SJAs command signal when $\alpha = 16$ degrees is crossed in the forward direction and vice versa. This is obtained by a control on the angle of attack derivative, $\dot{\alpha}$. The condition $\alpha = 16° \wedge \dot{\alpha} > 0$ activates the SJAs, and $\alpha = 16° \wedge \dot{\alpha} < 0$ deactivates them. The obtained lift coefficient vs. angle of attack line is shown in red in Figure 15. As expected the stall postposition effect is maintained where required without energy loss in the linear C_{L_α} region. This encouraging result motivates the authors to continue with further investigations in the attempt of activating the SJAs on a pressure reading on the wing.

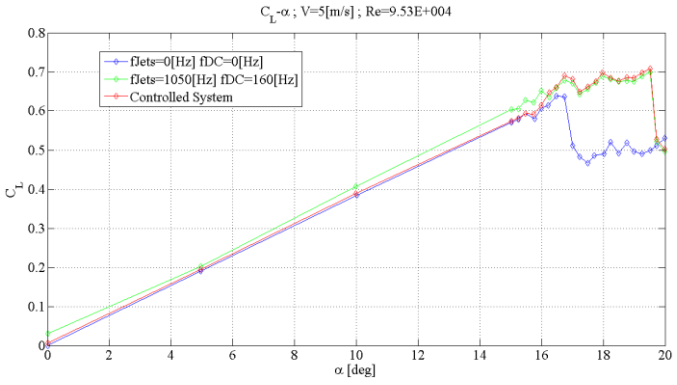

Figure 15 - Lift coefficient vs. AOA, Closed-loop control strategy compared to the open-loop

CONCLUSIONS

In the present paper the flow active control on a NACA 0015 wing section has been performed using two arrays of synthetic jet actuators. The tested configuration is characterized by a low aspect ratio wing in low Reynolds number flow conditions. The stall postposition has been the main objective of the SJAs application. Wind tunnel tests have been primarily performed in order to characterize and optimize the parameters related to the SJAs input signal. It has been observed that the sine-wave frequency is the most important parameter in defining the actuators effectiveness, compared to the bias voltage and duty cycle frequency. The second set of experiment validated the previous outcomes and allowed for aerodynamic database collection, both for the continuously actuated and non-actuated wing configurations. It has been demonstrated that a stall postponement of about 3 degrees is achieved with this configuration at a wind speed of $U_\infty = 5\ m/s$. In addition, the effect of the Reynolds number on the SJAs has been investigated in the second set of tests. The results have shown that higher Reynolds number reduces the SJAs effect and strongly affect the lift coefficient in a LAR wing because of the wing tip vortex effect. The third part of the experimental campaign has concerned the identification of a signature in the pressure distribution to be used as trigger for the active SJAs control. Three different methodologies has been applied leading to several interesting outcomes: the RMS analysis demonstrated a low fluctuation zone centered at about 38% of the chord which has been attributed to the laminar separation bubble, typical of the low Reynolds number flow configurations. The magnitude-squared coherence (MSC) demonstrated the existence of a definite structure of pressure fluctuations in the boundary layer in the chord-wise direction. The mean pressure approach demonstrated the feasibility of characterizing the streamline detachment by simple acoustic pressure transducer. Finally, a closed-loop control scheme has been designed and implemented using as feedback information the angle of attack provided by the balance system encoder. Stall postponement has been obtained only when required without energy loss in the linear C_{L_α} region. The encouraging results of the presented research motivates the authors to further investigation of SJAs active control based only on the acoustic pressure transducer measurements.

REFERENCES

[1]. Z.Wang, T.Hu, I.Gursul, *Active control of self-excited roll oscillations of LAR wings*. In: Zhou, Y., et al. Fluid-Structure-Sound Interactions and Control. [S.l.]: Springer, 2014.

[2]. Tovar, E. et al., *Networked Embedded Systems for Active Flow Control in Aircraft*. 11th International Workshop on Real Time Networks RTN. Pisa: [s.n.]. 2012.

[3]. Hubbard, J., Flatau, A., Clingman, D., *Phased Array Synthetic Jets For Influencing Dynamics Of Complex Flows.* Maryland, Us. 2014.

[4]. Tang, H. et al., *Active Flow Control Over a Wing Model Using Synthetic-Jet-Actuator Arrays*. In: Tang, H., et al. Fluid-Structure-Sound Interactions and Control. [S.l.]: Springer, 2014.

[5]. M.Stolk et al., *Active Flow and Aeroelastic Control of Lifting Surfaces Using Synthetic Jet Actuators*. SAE International, 2007.

[6]. Hong, G., *Effectiveness Of Micro Synthetic Jet Actuator Enhanced By Flow Instability*. [S.L.]. 2007.

[7]. Millar, A. C., *Flow Control Via Synthetic Jet Actuation.* Texas. 2004.

[8]. Alstrom, R. B., *Aerodynamic Flow Control Of A High Lift System With Dual Synthetic Jet Arrays.* [S.l.]. 2013.

[9]. Melton, L. P., Yao, C. S., *Active Control of Separation From the Flap of a Supercritical Airfoil.* [S.l.]. 2006.

[10]. Inman, D. J. et al., *Ducted Fan Aerodynamics and Modeling, with Applications of Steady and Synthetic Jet Flow Control***.** Blacksburg, VA, US. 2011.

[11]. Jabbal, M., Liddle, S.C., Crowther, W.J.,*Active Flow Control Systems Architectures For Civil Transport Aircraft.* Manchester. 2010.

[12]. Zeiger, M. D., Rediniotis, O. K., *Reconfigurable Synthetic Jet Actuation For Closed-Loop Hingeless Flow Control.* [S.L.]. 2004.

[13]. Golubev, V. V., Mackunis, W. *On Uav Robust Nonlinear Control.* ICAS. St. Petersburg: [s.n.]. 2014.

[14]. Neidhoefer, J., Ryan, J. C*ontinuing Experimental Development Of Hingeless Aerodynamic*. 27th AIAA Applied Aerodynamics Conference. San Antonio, Texas: [s.n.]. 2009.

[15]. Neidhoefer, J., *Development Of An Innovative Practical Uav With No Moving Aerodynamic Control Surfaces.* [S.l.]. 2006.

[16]. Lin, C. Y., Hsiao, F. B., *Experimental Study Of Flow Separation Over NACA633018 Wing With Synthetic Jet Control At Low Reynolds Numbers*. Journal Of Mechanics, 2012.

[17]. Cosyn, P., Vierendeels, J., *Numerical Investigation Of Low Aspect Ratio Wings At Low Reynolds Numbers*. Journal Of Aircraft, 2006.

[18]. Ikhlaq, M., Ghaffari, O., Arik, M., *Effect Of Actuator Deflection On Heat Transfer For Low And High Frequency Synthetic Jets*. Thermal and Thermomechanical Phenomena in Electronic Systems. Orlando, Florida, USA: IEEE. 2014.

[19]. Kabiri, P., *Active Flow Control Over A NACA0015 Airfoil By Synthetic Jet Actuators*. [S.l.]. 2012.

[20]. Noughabi, A. K., Tadjfar, M., *Cross-Wind Influence On Low Aspect Ratio Wings At Low Reynolds Numbers*. Asme 2013 Fluids Engineering Division Summer Meeting. Incline Village, Nevada, Usa: Asme. 2013.

[21]. Arivoli, D. et al., *Experimental Studies On A Propelled Micro Air Vehicle*. Aiaa Applied Aerodynamics Conference. Honolulu, Hawaii: [S.N.]. 2011.

[22]. Mueller, T. J., Torres, G. E., *Aerodynamics Of Low Aspect Ratio Wings At Low Reynolds Numbers With Applications To Micro Air Vehicles Design And Optimization*. [S.l.]. 2001.

[23]. Yang, H. H. Z., *An Experimental Study Of The Laminar Flow Separation On A Low-Reynolds Number-Airfoil*. Journal of Fluids Engineering, 2008.

[24]. Mansor, S. et al., *Flow Visualization And Measurement Of A Synthetic Jet Actuator Performance Using Piv System*. Journal Technology (Sciences & Engineering), 2014.

CONTACT INFORMATION

ACKNOWLEDGMENTS

The authors would like to thank the Clarkson University CAMP, Mechanical and Aeronautical Engineering Department, for making all the instrumentations available to conduct the research experiments.

DEFINITIONS/ABBREVIATIONS

LAR	Low Aspect Ratio
SJAs	Synthetic Jet Actuators
RMS	Root Mean Square
MSC	Magnitude Squared Coherence
AOA	Angle of Attack
q	Dynamic Pressure
Re	Reynolds number
$\boldsymbol{U}_{\infty}$	Free stream velocity